LA-UR-96- 2796

CONF-9609240--2

TITLE: Using BRDFs for Accurate Albedo Calculations and Adjacency Effect Corrections

AUTHOR(S): Christoph C. Borel
Siefgried A. W. Gerstl

SUBMITTED TO: International Workshop on Multiangular Remote Sensing: Measurements, Models, and Applications.
Institute of Remote Sensing Applications,
Chinese Academy of Sciences
Beijing China

Los Alamos
NATIONAL LABORATORY

VM

Form No. 836 R5
ST 2629 10/91

DISCLAIMER

USING BRDFs FOR ACCURATE ALBEDO CALCULATIONS AND ADJACENCY EFFECT CORRECTIONS

Christoph C. Borel, Siegfried A. W. Gerstl
NIS-2, Mailstop C323, Los Alamos National Laboratory, Los Alamos, NM 87545, USA
E-mail: cborel@lanl.gov; http://nis-www.lanl.gov/~borel/

Abstract

In this paper we will discuss two uses of BRDFs in remote sensing: (1) in determining the clear sky top of the atmosphere (TOA) albedo, (2) in quantifying the effect of the BRDF on the adjacency point-spread function and on atmospheric corrections.

The TOA spectral albedo is an important parameter retrieved by the Multi-angle Imaging Spectro-Radiometer (MISR). Its accuracy depends mainly on how well we can model the surface BRDF for many different situations. We will present results from an algorithm which matches several semi-empirical functions to the nine MISR measured BRFs that are then numerically integrated to yield the clear sky TOA spectral albedo in four spectral channels. We show that absolute accuracies in the albedo of better than 1 % are possible for the visible and better than 2 % in the near infrared channels.

Using a simplified extensive radiosity model, we will show that the shape of the adjacency point-spread function (PSF) depends on the underlying surface BRDFs. The adjacency point-spread function at a given offset (x,y) from the center pixel is given by the integral of transmission-weighted products of BRDF and scattering phase function along the line of sight.

1 TOA Albedo Algorithm based on Semi-Empirical Models

The Multi-angle Imaging Spectro-Radiometer (MISR) instrument is slated for the EOS-AM platform to be launched in 1998. The instrument consists of nine cameras pointed at zenith angles of ±70.5, ±60, ±45, ±26.1 and 0 degrees in the along track direction. Each camera has four spectral channels with center bandpass wavelengths at 443 nm (blue), 550 nm (green), 670 nm (red) and 865 nm (near infrared). The instrument will be used to infer top of the atmosphere spectral albedo (clear and cloudy conditions), surface bidirectional reflectance, global aerosol distributions and other atmosphere and surface parameters at the 4 spectral bands. Global monitoring of the earth radiation budget is one of the main goals in global change research programs.

1.1 Simulated MISR Data Set

Since there is no MISR data yet available it was necessary to simulate MISR data as closely as possible to what will be expected from the EOS instrument in a few years. Several "Radiative transfer" (RT) codes were considered for this task. A key requirement was that the surface had to be modeled using a surface "Bidirectional Reflectance Distribution Function" (BRDF) (e.g. Nicodemus et al, 1977). Furthermore the RT codes must accurately calculate the multiple scattering for a large range of sun and view angles in order to perform a numerical integration over the hemispherical BRF for the albedo calculation. Multiple scattering is an important component of the measured signal in the visible and near infrared spectral region.

Using a radiative transfer code written by John Martonchik at JPL we generated hemispherical TOA radiance fields for four MISR channels, five different aerosol types (urban, rural, maritime, desert and arctic) and 46 surface BRDFs from experimental data and models for vegetation (23), bare soil (3), rough water surface (11), snow and ice (9).

1.2 Semi-Empirical Models

Since MISR measures only in nine discrete directions it is necessary to estimate the TOA radiance in directions which are not seen by MISR using what we call an azimuthal model (AZM). Various Semi-Empirical Models (SEM) were considered in this study and used to compute an albedo estimate $\widehat{\alpha_{0,c}}$ for channel c. The basic idea is to take a semi-empirical function which is able to represent many different TOA BRFs. This function should have as few parameters as possible, is uniquely invertible, reciprocal (sun and view angles are interchangeable without changing the value) and should have little sensitivity to noise.

As a good starting point we decided to investigate the "Coupled Surface-Atmosphere Reflectance" (CSAR) model further, Rahman et al., 1993. Using the CSAR model worked well except for very dark surfaces. We found that including some atmospheric terms in the CSAR model improved the albedo estimates over dark surfaces. The modified CSAR model we used has the form:

$$BRF_{mod}(\theta_s, \phi_s; \theta_r, \phi_r; h) = BRF_{CSAR} * \exp(-\frac{\tau}{\mu_s} - \frac{\tau}{\mu_r}) + BRF_{Rayleigh}(\theta_s, \phi_s; \theta_r, \phi_r; h), \quad (1)$$

where the subscript s denotes the illumination direction, subscript r denotes the view direction, h is the altitude of the surface and τ is the optical depth. The Rayleigh path radiance is converted to a $BRF_{Rayleigh}$ and was computed using JMRT or a routine from 6S.

1.3 Algorithm Outline

The following algorithm was implemented and tested on simulated MISR BRFs over many surface types and atmospheric conditions:

1. Read TOA BRFs from JMRT output
2. For all N_K cases $k = 1, 2, 3, \ldots, N_K$ do:
   (a) Compute the albedo $\alpha_{0,k}$
   (b) For view azimuth angles $\phi_j = [0^o,\ 30^o,\ 60^o,\ 90^o]$ do:
      i. Extract a BRF slice ($BRF_i,\ i = 1, 2, \ldots, 9$) at the MISR angles for ($\phi_j,\ \phi_j + 180^o$).
      ii. Perform nonlinear curve fit of $BRF_{j,i}$ results in estimated CSAR parameters $\widehat{\varrho_{0,j,k}}$, $\widehat{\kappa_{j,k}}$ and $\widehat{\Theta_{0,j,k}}$.
      iii. Do a numerical integration of CSAR model over the hemisphere results in estimated albedo $\widehat{\alpha_{0,j,k}}$.
      iv. Compute albedo error $\varepsilon(\alpha_{0,j,k}) = \alpha_{0,k} - \widehat{\alpha_{0,j,k}}$.
   (c) Plot standard deviation σ of the albedo error $\varepsilon(\alpha_{0,j,k})$ as a function of view azimuth ϕ_j.
   (d) Generate TOA BRF from estimated CSAR parameters and display next to original.
3. Generate scatter plots of standard deviation of the albedo error versus azimuth marking different surface types with symbols.

1.4 Results

We find that for most cases our albedo error will be less than 1% in the visible and less than 1.5% in the NIR which is a significant advancement of the state-of-the-art for global change research goals. In contrast, if only nadir measurements are used the albedo error is about 5 % in the visible and 10 % in the NIR. More work is however needed to make this approach robustly work for all surfaces and atmospheric conditions. We found that it was possible to use retrieved model parameters in the NIR to distinguish vegetative from non-vegetative surfaces.

2 BRDF Dependent Adjacency Effect

When images of heterogeneous land surfaces are acquired through the atmosphere, the measured radiance data include not only the surface radiances per pixel but also contain modifications due to the atmosphere. Correcting such modified land imagery for atmospheric effects, one must consider atmospheric absorption as well as scattering. In this section we concentrate on the atmospheric scattering that gives rise to a blurring effect of adjacent pixels. One can model the blurring due to the adjacency effect with a point spread function (PSF). That PSF is a filter function which is convolved with the unperturbed (no atmosphere) image of a surface. Most PSF's are generated by Monte Carlo-based methods and are assumed to be rotationally symmetric and thus, are not valid for off-nadir views. In the situation of a pointable sensor, it is necessary to compute off-nadir PSF's which are generally asymmetric. Our simulation takes aerosol scattering phase functions and ground bidirectional reflectance distributions (BRDF) into account. Using the inverse filter of the PSF it is possible to correct the adjacency-blurred image and restore the unperturbed contrast ratios at reflectance discontinuities.

The extended radiosity method (Borel and Gerstl, 1991) is based on radiative transfer and considers energy exchange between volume/volume, volume/surface, surface/volume and surface/ surface elements. It assumes :

1. Isotropic, volumetric emission and scattering by the participating medium for the volume elements
2. Diffuse (Lambertian) reflection from opaque surfaces
3. Arbitrary directional illumination

The radiosities are given by the sums of the emission and the scattered and reflected radiosities from all other surfaces and volumes. The view factors are defined as the ratio of the total energy emitted or scattered by a surface or volume arriving at another surface or volume divided by the radiosity of the source surface or volume.

2.1 Point-Spread Function for Lambertian Surfaces

In an optical system the point spread function $PSF(x, y, z; x_0, y_0, z_0; \theta_s, \phi_s; \theta_r, \phi_r)$ can be defined as the scattering contribution of a surface element $dA = dx\ dy$ illuminated from direction (θ_s, ϕ_s) located at $(x, y, z = z_0)$ into the line-of-sight direction of the observer (θ_r, ϕ_r) looking at point (x_0, y_0, z_0). Figure 1 shows the geometry for the ground to atmosphere scattering. One can show (see Borel and Gerstl, 1992a and 1992b) that the unit less PSF is given by :

$$PSF(x, y, \ldots) = \frac{\kappa_s\ \Delta l}{4\ \pi} \sum_{k=1}^{K} \frac{\tau(r_k)\ \cos\theta_{r,k}\ f(\theta_{p,k})\ dx\ dy}{\pi\ r_k^2} \cdot \exp(-\kappa_t\ (K-k)\ \Delta l), \qquad (2)$$

where κ_s is the scattering coefficient in $[m^{-1}]$, $\Delta l = L_z/(K\cos\theta_r)$, L_z is the height of the scattering atmosphere, K is the number of layers in the atmosphere, $\tau(r_k) = \exp(-\kappa_t r_k)$, κ_t is the total scattering coefficient in $[m^{-1}]$, r_k is the distance between surface point $\vec{P}$ and a point $\vec{P_k}$ on the line-of-sight in the k-th layer, $\theta_{r,k}$ the view zenith angle to dA, $f(\theta_{p,k})$ is the scattering phase function of the k-th layer and $\theta_{p,k}$ is the scattering phase angle. Note that this method takes height dependent scattering and absorption coefficients and even height dependent scattering phase functions into account. The method can even be extended to include terrain effects when the PSF is computed for each pixel in the scene. For the Lambertian surface the PSF for nadir view is rotationally symmetric and asymmetric for all non-nadir views.

According to Borel and Gerstl, 1992a, the measured radiance $I_{measured}(x, y, z; x_0, y_0, z_0; \theta_s, \phi_s;\ \theta_r, \phi_r)$ in $[W\ m^{-2}]$ at the sensor for a Lambertian surface is given by :

$$I_{measured}(x, y, \ldots) \ = \ \frac{E_0}{\pi}\tau_s\Big[T_r\rho(x_0, y_0) \ + \ \rho(x, y) \otimes PSF(x, y, \ldots)\Big] \ + \ I_{path} \tag{3}$$

where E_0 is the direct energy incident from the sun in $[W\ m^{-2}]$, $\tau_s = \exp(-\kappa_t L_z/\cos\theta_s)$, $T_r = \exp(-\kappa_t L_z/\cos\theta_r)$, $\rho(x, y)$ is the reflectance at point (x, y), $\otimes$ denotes the convolution and I_{path} is the path radiance or radiance due to scattering in the atmosphere.

2.2 Point-Spread Function for Non-Lambertian Surfaces

In practical situations the imaged ground surface is non-Lambertian and thus the above described method may lead to inaccurate simulated images. We attempt now to include the bidirectional reflectance distribution function (BRDF) in the computation of the PSF. First, let us assume that the entire surface has the BRDF :

$$f(x, y, z; \theta_s, \phi_s; \theta_r, \phi_r) = f(\theta_s, \phi_s; \theta_r, \phi_r).$$

Second, that the contributions from indirect skylight are negligible on the radiance in direction $(\theta_{r,k}, \phi_{r,k})$ or that the upwelling radiance I_{ground} at the ground level is proportional to $f(\theta_s, \phi_s; \theta_r, \phi_r)$. This second assumption clearly is not valid for turbid atmospheres and for highly specular surfaces like water. Under these two assumptions we can replace $\rho(x, y)$ in eq (2) with $\pi f(\theta_s, \phi_s; \theta_r, \phi_r)$. Note that BRDFs for natural surfaces are usually asymmetric and cause the PSF to be asymmetric for all view directions, including nadir. The PSF for non-Lambertian surfaces is then given by :

$$PSF(x, y, \ldots) \ = \ \frac{\kappa_s\ \Delta l}{4\ \pi}\ \sum_{k=1}^{K}\ \frac{\tau(r_k)\ f(\theta_s, \phi_s; \theta_{r,k}, \phi_{r,k})\cos\theta_{r,k}\ f(\theta_{p,k})\ dx\ dy}{r_k^2}\exp(-\kappa_t(K-k)\Delta l), \tag{4}$$

where $\phi_{r,k}$ is the view azimuth angle of surface dA from point $\vec{P_k}$.

2.3 Simulation of Scenes with Heterogeneous Surface Cover

The Earths, surface is composed of a mosaic of various surface types such as vegetation, bare soil and water, each with distinct BRDFs. To simulate an oblique view over a heterogeneous surface the following algorithm was used :

1. For each surface BRDF $f_i(\theta_s, \phi_s; \theta_r, \phi_r),\ i = 1, 2, \ldots, N$ compute the point spread function $PSF_i(x, y, \ldots)$ using eq (4).
2. Generate a binary image $Q_i(x, y)$ for each surface type i, where $Q_i(x, y) = 1$ if the point (x, y) has surface cover type i and 0 otherwise.

3. Convolve each image $Q_i(x,y)$ with its point spread function $PSF_i(x,y,\ldots)$.

The measured radiance image is then given by :

$$I_{measured}(x,y) = \frac{E_0}{\pi}\tau_s \sum_{i=1}^{N}\Big[T_r Q_i(x_0,y_0) f_i(\theta_s,\phi_s;\theta_r,\phi_r) + Q_i(x,y) \otimes PSF_i(x,y,\ldots)\Big] + I_{path}. \quad (5)$$

Equation (5) shows that the adjacency blurring effect is the superposition of ground cover type images convolved with their corresponding point spread functions.

In Figure 2 we show the point spread functions for (a) bare soil, (b) vegetation and (c) water. Note that the PSF's are asymmetric and that the PSF for water has a ridge in the specular reflection direction (left side) of the sun which has a zenith angle of 30^0.

3 Conclusions

We find that for most cases our albedo error will be less than 1% in the visible and less than 1.5% in the NIR which is a significant advancement of the state-of-the-art for global change research goals. In contrast, if only nadir measurements are used the albedo error is about 5 % in the visible and 10 % in the NIR. Thus the angular dependence of the TOA radiance which depends on the surface BRDF is an important factor in the determination of TOA albedos for clear sky conditions. Next we will investigate how the CSAR parameters vary as a function of sun angle. If we find that there is a diurnal smooth trajectory for a parameter with sun angle we could use this to predict the TOA clear sky albedo at times of the day other than those at which MISR observed it and integrate the TOA albedo over the period of a day.

We have presented a method to compute the point spread function for off-nadir pointing sensors using selected parts of the radiosity equation. We showed that the point spread function is in general asymmetric. The radiosity based method is able to include surface BRDF, aerosol scattering phase functions and atmospheric parameters for a stratified atmosphere. The adjacency blurring effect was simulated for a scene containing vegetated, bare soil and water surfaces. Thus knowledge of the surface BRDFs could lead to improved atmospheric corrections of VIS/NIR imagery over heterogeneous covers.

4 References

Borel C.C. and Gerstl S.A.W., 1991, Simulation of Partially Obscured Scenes Using the Radiosity Method, SPIE Technical Symp. on Opt. Eng. and Phot. in Aerosp. Sens., Orlando, Vol.1486, FL, April 1-5, pp. 271-277.

Borel C.C. and Gerstl S.A.W., 1992a, Atmospheric Corrections using the Volume Radiosity Method, Proc. of IGARSS'92, p.1231-1234.

Borel C.C. and Gerstl S.A.W., 1992b, Adjacency-Blurring-Effect of Scenes Modeled by the Radiosity Method, Proc. SPIE'92, Vol. 1688, pp.620-624.

Nicodemus F.E., Richmond J.C., Hsia J.J., Ginsberg I.W. and Limperis T., 1977, Geometrical Considerations and Nomenclature for Reflectance, Washington, D.C.: NBS Monograph 160, National Bureau of Standards, Dept. of Commerce, p.52.

Rahman H., Verstraete M.M. and Pinty B., 1993, Coupled Surface- Atmosphere Reflectance (CSAR) Model (parts 1 and 2), JGR, 98:D11:20,779-20,789 and 98:D11:20,791-20,801.

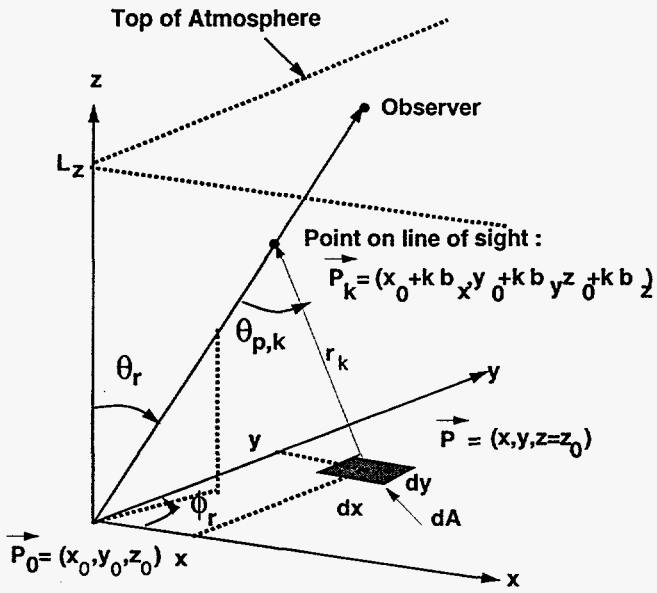

Figure 1 Geometry for computing the point spread function.

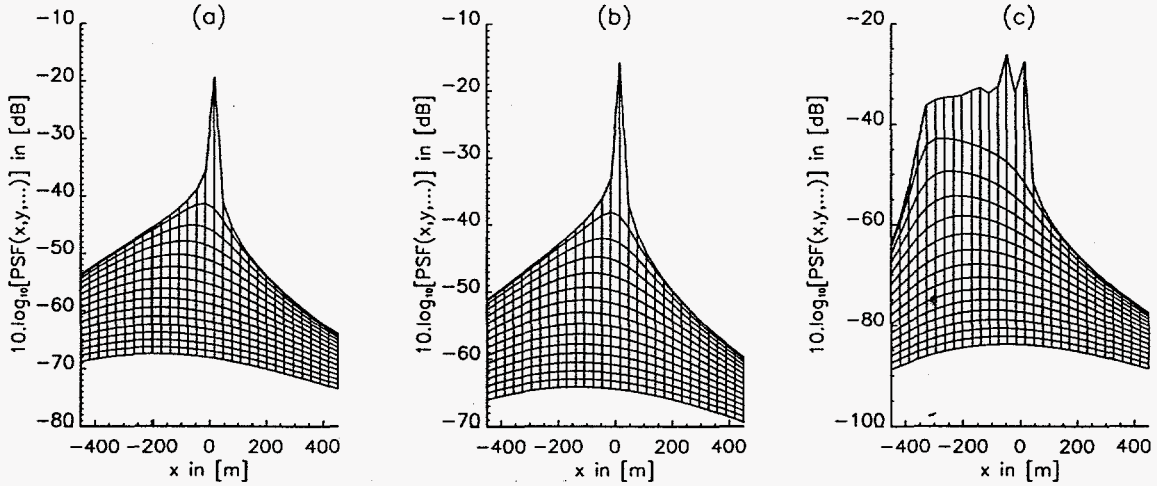

Figure 2 Point spread functions of (a) bare soil, (b) vegetation and (c) water with the z-axis in logarithmic scale and the y-axis points into the paper.